

Spectral energy dynamics in magnetohydrodynamic turbulence

Wolf-Christian Müller

Max-Planck-Institut für Plasmaphysik, 85748 Garching, Germany

Roland Grappin

Observatoire de Paris-Meudon, 92195 Meudon, France

Spectral direct numerical simulations of incompressible MHD turbulence at a resolution of up to 1024^3 collocation points are presented for a statistically isotropic system as well as for a setup with an imposed strong mean magnetic field. The spectra of residual energy, $E_k^R = |E_k^M - E_k^K|$, and total energy, $E_k = E_k^K + E_k^M$, are observed to scale self-similarly in the inertial range as $E_k^R \sim k^{-7/3}$, $E_k \sim k^{-5/3}$ (isotropic case) and $E_{k_\perp}^R \sim k_\perp^{-2}$, $E_{k_\perp} \sim k_\perp^{-3/2}$ (anisotropic case, perpendicular to the mean field direction). A model of dynamic equilibrium between kinetic and magnetic energy, based on the corresponding evolution equations of the eddy-damped quasi-normal Markovian (EDQNM) closure approximation, explains the findings. The assumed interplay of turbulent dynamo and Alfvén effect yields $E_k^R \sim k E_k^2$ which is confirmed by the simulations.

The nonlinear behavior of turbulent plasmas gives rise to a variety of dynamical effects such as self-organization of magnetic confinement configurations in laboratory experiments [1], generation of stellar magnetic fields [2] or structure formation in the interstellar medium [3]. The understanding of these phenomena is incomplete as the same is true for many inherent properties of the underlying turbulence.

Large-scale low-frequency plasma turbulence is treated in the magnetohydrodynamic (MHD) approximation describing the medium as a viscous and electrically resistive magnetofluid neglecting additional kinetic effects. Incompressibility of the flow is assumed for the sake of simplicity. In this setting the nature of the turbulent energy cascade is a central and still debated issue with different phenomenologies being proposed [4, 5, 6, 7, 8] (cf. [9] for a review). The associated spectral dynamics of kinetic and magnetic energy, in spite of its comparable importance, has received less attention (as an exception see [10]).

This Letter reports a spectral relation between residual and total energy, $E_k^R = |E_k^M - E_k^K|$ and $E_k = E_k^K + E_k^M$ respectively, as well as the influence of an imposed mean magnetic field on the spectra. The proposed physical picture, which is confirmed by accompanying direct numerical simulations, embraces two-dimensional MHD turbulence, globally isotropic three-dimensional systems as well as turbulence permeated by a strong mean magnetic field.

In the following reference is made to two high-resolution pseudospectral direct numerical simulations of incompressible MHD turbulence which we regard as paradigms for isotropic (I) and anisotropic (II) MHD turbulence. The dimensionless MHD equations

$$\partial_t \boldsymbol{\omega} = \nabla \times [\mathbf{v} \times \boldsymbol{\omega} - \mathbf{b} \times (\nabla \times \mathbf{b})] + \mu \Delta \boldsymbol{\omega} \quad (1)$$

$$\partial_t \mathbf{b} = \nabla \times (\mathbf{v} \times \mathbf{b}) + \eta \Delta \mathbf{b} \quad (2)$$

$$\nabla \cdot \mathbf{v} = \nabla \cdot \mathbf{b} = 0. \quad (3)$$

are solved in a 2π -periodic cube with spherical mode truncation to reduce numerical aliasing errors [11]. The equations include the flow vorticity, $\boldsymbol{\omega} = \nabla \times \mathbf{v}$, the magnetic field expressed in Alfvén speed units, \mathbf{b} , as well as dimensionless viscosity, μ , and resistivity, η . In simulation II forcing is applied by freezing the largest spatial scales of velocity and magnetic field.

Simulation I evolves globally isotropic freely decaying turbulence represented by 1024^3 Fourier modes. The initial fields are smooth with random phases and fluctuation amplitudes following $\exp(-k^2/(2k_0^2))$ with $k_0 = 4$. Total kinetic and magnetic energy are initially equal with $E^K = E^M = 0.5$. The ratio E^K/E^M decreases in time taking on values of $0.28 - 0.23$ in the period considered (cf. [12]). The ratio of kinetic and magnetic energy dissipation rate, $\varepsilon^K/\varepsilon^M$, with $\mu = \eta = 1 \times 10^{-4}$ also decreases during turbulence decay from 0.7 to about 0.6 , the difference in dissipation rates reflecting the imbalance of the related energies. The Reynolds number $\text{Re} = (E^K)/(\mu \varepsilon^{\text{total}})$ at $t = 6$ is about 2700 and slightly diminishes during the run. Magnetic, $H^M = \frac{1}{2} \int_V dV \mathbf{a} \cdot \mathbf{b}$, $\mathbf{b} = \nabla \times \mathbf{a}$, and cross helicity, $H^C = \frac{1}{2} \int_V dV \mathbf{v} \cdot \mathbf{b}$, are negligible with H^C showing a dynamically unimportant increase from 0.03 to 0.07 during the simulation. The run covers 9 eddy turnover times defined as the time required to reach the maximum of dissipation from $t = 0$. The large-scale rms magnetic field decays from initially 0.7 to 0.3 .

Case II is a $1024^2 \times 256$ forced turbulence simulation with an imposed constant mean magnetic field of strength $b_0 = 5$ in units of the large-scale rms magnetic field $b_{\text{rms}} \simeq v_{\text{rms}} \simeq 1$. The forcing, which keeps the ratio of fluctuations to mean field approximately constant, is implemented by freezing modes with $k \leq k_f = 2$. The simulation with $\mu = \eta = 9 \times 10^{-5}$ has been brought into quasi-equilibrium over 20 eddy-turnover times at a resolution of $512^2 \times 256$ and spans about 5 eddy turnover times of quasi-stationary turbulence with $1024^2 \times 256$

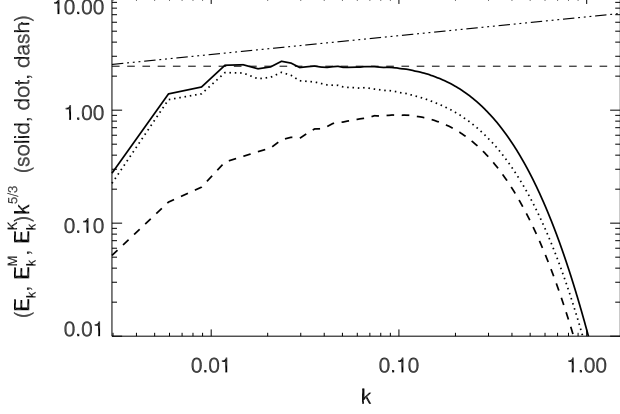


FIG. 1: Total (solid), kinetic (dashed), and magnetic (dotted) energy spectra in 1024^3 case I simulation (normalized, time-averaged and compensated). Dash-dotted line: $k^{-3/2}$ scaling.

Fourier modes and $\text{Re} \approx 2300$ (based on field perpendicular fluctuations). Kinetic and magnetic energy as well as the ratio E^K/E^M are approximately unity with a slight excess of E^M . Perpendicular to the imposed field, large-scale magnetic fluctuations with $b_{\text{rms}} \simeq 0.4$ are observed. Correspondingly, $\varepsilon^K/\varepsilon^M \simeq 0.95$ during the simulation. The system has relaxed to $H^C \simeq 0.15$ with a fluctuation level of about 30% and $H^M \simeq 0.2H_{\text{Max}}^M$ with $H_{\text{Max}}^M \sim E^M/k_f$.

Fourier-space-angle integrated spectra of total, magnetic, and kinetic energy for case I are shown in Fig. 1. To neutralize secular changes as a consequence of turbulence decay, amplitude normalization is used assuming a Kolmogorov total energy spectrum, $E_k \rightarrow E_k/(\varepsilon\mu^5)$, $\varepsilon = -\partial_t E$, with wavenumbers given in inverse multiples of the associated dissipation length, $\ell_D \sim (\mu^3/\varepsilon)^{1/4}$. The quasi-stationary normalized spectra are time averaged over the period of self-similar decay, $t = 6 - 8.9$. As in previous numerical work [13, 14] and also observed in solar wind measurements [15, 16], Kolmogorov scaling applies for the total energy in the well-developed inertial range, $0.01 \lesssim k \lesssim 0.1$. However, here the remarkable growth of excess magnetic energy with decreasing wavenumber is of interest. Qualitatively similar behavior is observed with large scale forcing exerted on the system. We note that no pile-up of energy is seen at the dissipative fall-off contrary to other high-resolution simulations [14, 17]. Apart from different numerical techniques and physical models this difference might be due to the limited simulation period at highest resolution namely 5 [14] and 4.3 [17] large-eddy-turnover times. Depending on initial conditions the energy spectrum at 1024^3 -resolution is still transient at that time.

In case II, pictured in Fig. 2, strong anisotropy is generated due to turbulence depletion along the mean

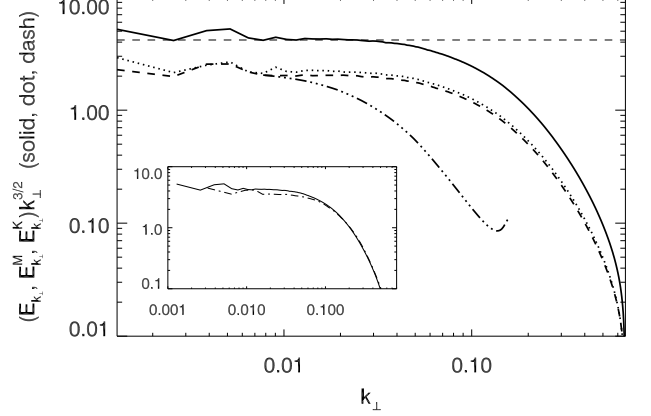


FIG. 2: Field-perpendicular total (solid), kinetic (dashed), and magnetic (dotted) energy spectra (normalized, time-averaged, and compensated) in $1024^2 \times 256$ case II simulation with $b_0 = 5$. Dash-dotted curve: high-k part of field-parallel total energy spectrum. Inset: perpendicular total energy spectrum for resolutions of 512^2 (dash-dotted) to 1024^2 (solid).

magnetic field, \mathbf{b}_0 , (cf. also [18, 19, 20, 21, 22]). This is visible when comparing the normalized and time-averaged field-perpendicular one-dimensional spectrum, $E_{k_\perp} = \int \int dk_1 dk_2 E(k_\perp, k_1, k_2)$ (solid line) with the field-parallel spectrum, defined correspondingly and adumbrated by the dash-dotted line in Fig. 2. The fixed k_\perp -axis is chosen arbitrarily in the k_1 - k_2 -plane perpendicular to \mathbf{b}_0 where fluctuations are nearly isotropic. For the strong b_0 chosen here, field-parallel and -perpendicular energy spectra do not differ notably from the ones found by considering the direction of the local magnetic field as done e.g. in [18, 23]. The field-parallel dissipation length is larger than in field-perpendicular directions because of the stiffness of magnetic field lines. The numerical resolution in the parallel direction can, therefore, be reduced.

While there is no discernible inertial range in the parallel spectrum, its perpendicular counterpart exhibits an interval with Iroshnikov-Kraichnan scaling, $E_{k_\perp} \sim k_\perp^{-3/2}$ (Note that due to identical energy scales in Figs. 1 and 2 the absolute difference between Kolmogorov and Iroshnikov-Kraichnan scaling is the same as in Fig.1). This is in contradiction to the anisotropic cascade phenomenology of Goldreich and Sridhar for strong turbulence predicting $E_{k_\perp} \sim k_\perp^{-5/3}$ [7] and with numerical studies claiming to support the GS picture [23, 24]. However, the strength of \mathbf{b}_0 in these simulations is of the order of the turbulent fluctuations and consequently much weaker than for the anisotropic system considered here. We note that indication for field-perpendicular IK scaling has been obtained in earlier simulations at lower resolution using a high-order hyperviscosity and with a stronger

mean component, $b_0/b \sim 3 \times 10^2$ [25]. The authors of the aforementioned paper, however, are unsure whether they observe a numerical artefact or physical behavior.

The strongly disparate spectral extent of field-parallel and -perpendicular fluctuations suggests that Alfvén waves propagating along the mean field do not have a significant influence on the perpendicular energy spectrum (in the sense of Goldreich-Sridhar, cf. also [21]). Instead, the strong \mathbf{b}_0 constrains turbulence to quasi-two-dimensional field-perpendicular planes as is well known and has been shown for this particular system [18].

Another intriguing feature of system II is that $E_k^K \simeq E_k^M$ with only slight dominance of E^M (cf. Fig. 2) in contrast to the growing excess of spectral magnetic energy with increasing spatial scale for case I. Since both states are dynamically stable against externally imposed perturbations (as has been verified numerically), they presumably represent equilibria between two competing nonlinear processes: field-line deformation by turbulent motions on the spectrally local time scale $\tau_{NL} \sim \ell/v_\ell \sim (k^3 E_k^K)^{-1/2}$ leading to magnetic field amplification (turbulent small-scale dynamo) and energy equipartition by shear Alfvén waves with the characteristic time $\tau_A \sim \ell/b_0 \sim (kb_0)^{-1}$ (Alfvén effect). The conjecture can be verified via the EDQNM closure approximation [26] which yields evolution equations for kinetic and magnetic energy spectra [27] by including a phenomenological eddy-damping term for third-order moments. The spectral evolution equation for the signed [32] residual energy, $E^R = E^M - E^K$, in the case of negligible cross helicity reads [28]:

$$(\partial_t + (\mu + \eta)k^2)E_k^R = \int_{\Delta} dp dq \Theta_{kpq} (T_{res}^R + T_{crs}^R + T_{Dyn}^R) \hat{1}$$

with the spectral energy flux contributions

$$\begin{aligned} T_{res}^R &= m_{kpq} \frac{k^2}{p} E_p^R E_q^R + r_{kpq} \frac{p^2}{q} E_q^R E_k^R, \\ T_{crs}^R &= -m_{kpq} p E_q E_k^R - t_{kpq} p E_q^R E_k, \\ T_{Dyn}^R &= \frac{s_{kpq}}{k} (k^2 E_p E_q - p^2 E_q E_k). \end{aligned}$$

The geometric coefficients m_{kpq} , r_{kpq} , s_{kpq} , t_{kpq} , a consequence of the solenoidality constraints (3), are given in [28]. The ‘ Δ ’ restricts integration to wave vectors \mathbf{k} , \mathbf{p} , \mathbf{q} which form a triangle, i.e. to a domain in the p - q plane which is defined by $q = |\mathbf{p} + \mathbf{k}|$. The time Θ_{kpq} is characteristic of the eddy damping of the nonlinear energy flux involving wave numbers k , p , and q . It is defined phenomenologically but its particular form does not play a role in the following arguments.

Local triad interactions with $k \sim p \sim q$ are dominating the hydrodynamic turbulent energy cascade and lead to Kolmogorov scaling of the associated spectrum (cf., for example, [29]). In contrast, the nonlinear interaction of Alfvén waves includes non-local triads with, e.g., $k \ll p \sim q$. In this case a simplified version of equation (4)

can be derived:

$$\partial_t E_k^R = -\Gamma_k k E_k^R \equiv T_{Alf}^R, \quad (5)$$

with $\Gamma_k = \frac{4}{3}k \int_0^{ak} dq \Theta_{kpq} E_q^M$ [27] $\sim k E^M \Theta$.

It is now assumed that the right hand side of (4) can be written as $T_{Alf}^R + T_{Dyn}^R$ [10]. This states that the residual energy is a result of a dynamic equilibrium between turbulent dynamo and Alfvén effect. For stationary conditions and in the inertial range, dimensional analysis of (4) and (5) yields $k^3 E_k^2 \sim k^2 E^M E_k^R$ which can be rewritten as

$$E_k^R \sim k E_k^2. \quad (6)$$

The relaxation time, Θ , appears as a factor on both sides of the relation and, consequently, drops out. We note that with $\tau_A \sim (kb_0)^{-1}$, where b_0 is the mean magnetic field carried by the largest eddies, $b_0 \sim (E^M)^{1/2}$, and by re-defining $\tau_{NL} \sim \ell/(v_\ell^2 + b_\ell^2)^{1/2} \sim (k^3 E_k)^{-1/2}$ (for system II all involved quantities are based on field-perpendicular fluctuations) relation (6) can be obtained in the physically more instructive form

$$E_k^R \sim \left(\frac{\tau_A}{\tau_{NL}} \right)^2 E_k. \quad (7)$$

The modification of τ_{NL} is motivated by considering that gradients of the Alfvén speed contribute to nonlinear transfer as much as velocity shear (see, e.g., [30]).

For the examined setups relation (7) is consistent with the underlying physical idea of dynamical equilibrium between Alfvén and dynamo effect. At small scales with $k \gg k_0$ (for system II: $k_0 \simeq k_f$), Alfvénic interaction always dominates the energy exchange since $\tau_A \ll \tau_{NL}$ (e.g. at $k = 0.3 l_D^{-1}$ for system I: $\tau_A \simeq 5 \times 10^{-2}$, $\tau_{NL} \simeq 0.2$, for system II: $\tau_A \simeq 1 \times 10^{-2}$, $\tau_{NL} \simeq 0.1$) which results in approximate spectral equipartition of kinetic and magnetic energy. At larger spatial scales the Alfvén effect becomes less efficient in balancing the transformation of kinetic to magnetic energy by the small-scale dynamo with $\tau_A \simeq \tau_{NL}$ (e.g. at $k = 0.01 l_D^{-1}$ for system I: $\tau_A \simeq 0.9$, $\tau_{NL} \simeq 0.8$, at $k = 3 \times 10^{-3} l_D^{-1}$ for system II: $\tau_A \simeq 1.2$, $\tau_{NL} \simeq 0.9$) allowing larger deviations from equipartition.

An interesting consequence of (6) is that the difference between possible spectral scaling exponents, which is typically small and hard to measure reliably, is enlarged by a factor of two in E_k^R . Even with the limited Reynolds numbers in today’s simulations such a magnified difference is clearly observable (e.g. dash-dotted lines in Figs. 1 and 3). For system I with Kolmogorov scaling, $E_k \sim k^{-5/3}$ (Fig. 1), relation (6) predicts $E_k^R \sim k^{-7/3}$ in agreement with the simulation (Fig. 3). In the case of Iroshnikov-Kraichnan behavior, $E_{k_\perp} \sim k_\perp^{-3/2}$ as realized in system II (Fig. 2), $E_{k_\perp}^R \sim k_\perp^{-2}$ is obtained. This result is confirmed by the residual energy spectrum shown in

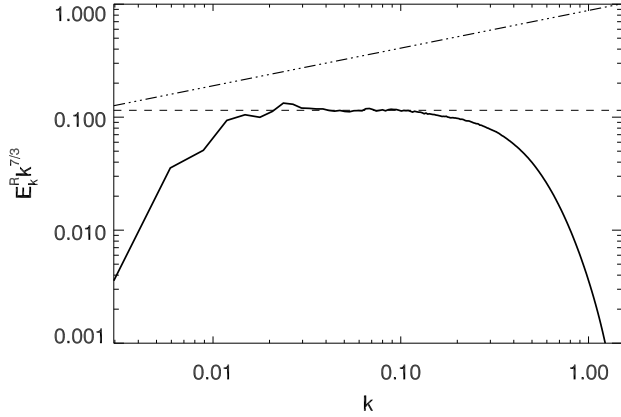


FIG. 3: Compensated, space-angle-integrated residual energy spectrum, E_k^R , for same system as in Fig. 1. Dash-dotted line: k^{-2} -scaling.

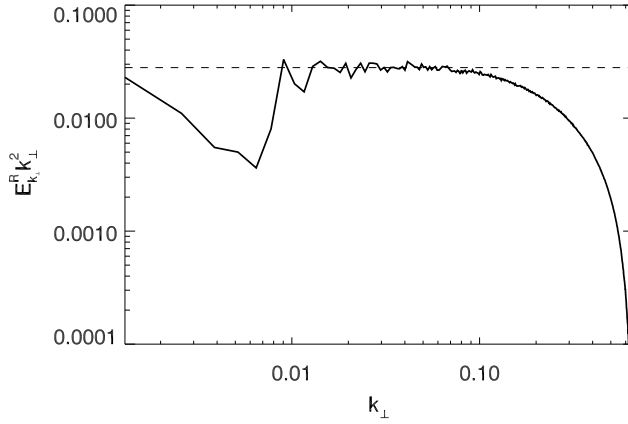


FIG. 4: Compensated field-perpendicular residual energy spectrum for the same system as in Fig. 2.

Fig. 4 (cf. also [31] for two-dimensional MHD simulations and [10] for spectral model calculations).

In summary, based on the structure of the EDQNM closure equations for incompressible MHD a model of the nonlinear spectral interplay between kinetic and magnetic energy is formulated. Throughout the inertial range a quasi-equilibrium of turbulent small-scale dynamo and Alfvén effect leads to the relation, $E_k^R \sim k E_k^2$, linking total and residual energy spectra, in particular $E_k^R \sim k^{-7/3}$ for $E_k \sim k^{-5/3}$ and $E_k^R \sim k^{-2}$ for $E_k \sim k^{-3/2}$. Both predictions are confirmed by high-resolution direct numerical simulations, limiting the possible validity of the Goldreich-Sridhar phenomenology to MHD turbulence with moderate mean magnetic fields.

The authors would like to thank Jacques Léorat and Dieter Biskamp for helpful discussions. WCM acknowl-

edges financial support by the CNRS and CIAS, Paris Observatory.

-
- [1] S. Ortolani and D. D. Schnack, *Magnetohydrodynamics of Plasma Relaxation* (World Scientific, Singapore, 1993).
 - [2] Y. B. Zeldovich, A. A. Ruzmaikin, and D. D. Sokoloff, *Magnetic Fields In Astrophysics* (Gordon and Breach Science Publishers, New York, 1983).
 - [3] D. Biskamp, *Magnetohydrodynamic Turbulence* (Cambridge University Press, Cambridge, 2003).
 - [4] A. N. Kolmogorov, Proceedings of the Royal Society A **434**, 9 (1991), [Dokl. Akad. Nauk SSSR, 30(4), 1941].
 - [5] P. S. Iroshnikov, Soviet Astronomy **7**, 566 (1964), [Astron. Zh., 40:742, 1963].
 - [6] R. H. Kraichnan, Physics of Fluids **8**, 1385 (1965).
 - [7] P. Goldreich and S. Sridhar, Astrophysical Journal **485**, 680 (1997).
 - [8] S. Sridhar and P. Goldreich, Astrophysical Journal **432**, 612 (1994).
 - [9] W.-C. Müller and D. Biskamp, in *Turbulence and Magnetic Fields in Astrophysics*, edited by E. Falgarone and T. Passot (Springer Berlin, 2002), vol. 614 of *Lecture Notes in Physics*, pp. 3–27.
 - [10] R. Grappin, A. Pouquet, and J. Léorat, Astronomy and Astrophysics **126**, 51 (1983).
 - [11] A. Vincent and M. Meneguzzi, Journal of Fluid Mechanics **225**, 1 (1991).
 - [12] D. Biskamp and W.-C. Müller, Physical Review Letters **83**, 2195 (1999).
 - [13] W.-C. Müller and D. Biskamp, Physical Review Letters **84**, 475 (2000).
 - [14] N. E. L. Haugen, A. Brandenburg, and W. Dobler, Physical Review E **70**, 016308 (2004).
 - [15] R. J. Leamon, C. W. Smith, N. F. Ness, W. H. Matthaeus, and H. K. Wong, Journal of Geophysical Research **103**, 4775 (1998).
 - [16] M. L. Goldstein and D. A. Roberts, Physics of Plasmas **6**, 4154 (1999).
 - [17] Y. Kaneda, T. Ishihara, M. Yokokawa, K. Itakura, and A. Uno, Physics of Fluids **15**, L21 (2003).
 - [18] W.-C. Müller, D. Biskamp, and R. Grappin, Physical Review E **67**, 066302 (2003).
 - [19] R. Grappin, Physics of Fluids **29**, 2433 (1986).
 - [20] J. V. Shebalin, W. H. Matthaeus, and D. Montgomery, Journal of Plasma Physics **29**, 525 (1983).
 - [21] R. M. Kinney and J. C. McWilliams, Physical Review E **57**, 7111 (1998).
 - [22] S. Oughton, W. H. Matthaeus, and S. Ghosh, Physics of Plasmas **5**, 4235 (1998).
 - [23] J. Cho, A. Lazarian, and E. T. Vishniac, Astrophysical Journal **564**, 291 (2002).
 - [24] J. Cho and E. T. Vishniac, Astrophysical Journal **539**, 273 (2000).
 - [25] J. Maron and P. Goldreich, Astrophysical Journal **554**, 1175 (2001).
 - [26] S. A. Orszag, Journal of Fluid Mechanics **41**, 363 (1970).
 - [27] A. Pouquet, U. Frisch, and J. Léorat, Journal of Fluid Mechanics **77**, 321 (1976).
 - [28] R. Grappin, U. Frisch, J. Léorat und A. Pouquet, Astronomy and Astrophysics **105**, 6 (1982).

- [29] M. Lesieur, *Turbulence in Fluids* (Kluwer Academic Publishers, Dordrecht, 1997).
- [30] J. Heyvaerts and E. R. Priest, *Astronomy & Astrophysics* **117**, 220 (1983).
- [31] D. Biskamp, *Chaos, Solitons & Fractals* **5**, 1779 (1995).
- [32] The other definition of E_k^R involving the modulus op-

erator avoids case differentiations since the applied dimensional analysis is unable to predict the sign of E^R . However, the physical picture underlying Eqs. (6) and (7) implies $E_k^M \geq E_k^K$ as it expresses an equilibrium between magnetic energy amplification and equipartition of E^K and E^M .